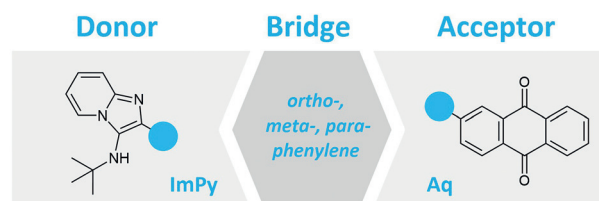# Design of Imidazo[1,2-*a*]pyridine-Based Donor–Acceptor Chromophores through a Multicomponent Approach

Mareen Stahlberger[a]

Milada Mergel[a]

John Marques dos Santos[b]

Tomas Matulaitis[b]

Martin Nieger[c]

Eli Zysman-Colman*[b]

Stefan Bräse*[a,d]

[a] Institute of Organic Chemistry (IOC), Karlsruhe Institute of Technology (KIT), Kaiserstrasse 12, 76131 Karlsruhe, Germany

[b] Organic Semiconductor Centre, EaStCHEM School of Chemistry, University of St Andrews, St Andrews, Fife, KY16 9ST, UK
eli.zysman-colman@st-andrews.ac.uk

[c] Department of Chemistry University of Helsinki, P. O. Box 55, 00014 University of Helsinki, Finland

[d] Institute of Biological and Chemical Systems Functional Molecular Systems (IBCS-FMS), Karlsruhe Institute of Technology (KIT), Kaiserstrasse 12, 76131 Karlsruhe, Germany
braese@kit.edu

Published as part of the Cluster
Chemical Synthesis and Catalysis in Germany
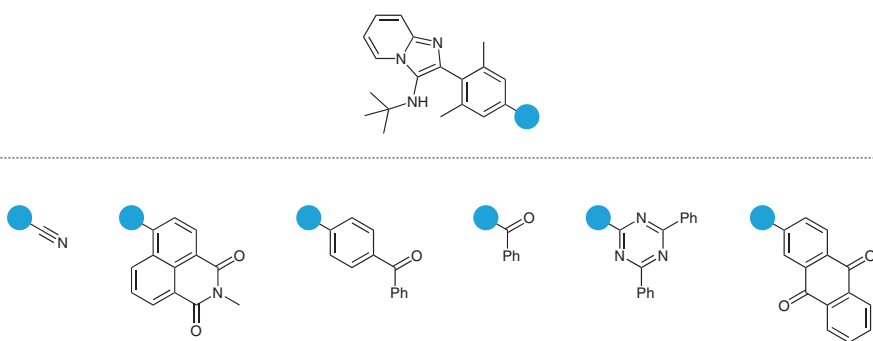
Abstract A series of donor-acceptor chromophores was synthesized bearing a 3-aminoimidazo[1,2-*a*]pyridine donor motive. Through DFT calculations, different combinations of the ImPy donor motive and different electron acceptors were assessed. In combination with an anthraquinone acceptor, the calculated ΔE_{ST} values were in range to suggest that these compounds would emit *via* thermally activated delayed fluorescence. Based on these findings, a series of ImPy-Aq emitters with different geometries and substitution patterns was synthesized through GBB-3CR and Suzuki coupling reactions. According to preliminary experimental data, the compounds were only slightly emissive at ambient temperatures due to a combination of low radiative rates and competing non-radiative deactivation pathways.

Key words multicomponent reaction, imidazo[1,2-*a*]pyridine, Suzuki coupling, thermally activated delayed fluorescence, donor-acceptor chromophores

Imidazo[1,2-*a*]heterocyclic scaffolds are well-explored substrates in medicinal chemistry while examples of their application in material science remain relatively scarce.[1] However, the intrinsic fluorescence of imidazopyridine (ImPy) and related fused systems is quite intriguing and could be very promising for the development of novel fluorophores.[2] ImPys are easily accessible through an isonitrile-based multicomponent reaction (MCR), the Groebke–Black-burn–Bienaymé reaction (GBB-3CR).[3] The modular nature of MCRs would also allow for easy assembly, customization and fine-tuning of the optoelectronic properties of these compounds.[4] However, possible applications of the GBB-3CR and its products for the design of functional chromophores have not been explored thoroughly. One of the few examples of the synthesis of chromophores based on the GBB-3CR was reported by Burchak *et al.* in 2011.[5] Shahrisa *et al.* reported a library of donor-acceptor fluorophores consisting of imidazo[1,2-*a*]pyridines as donors in combination with tetrazole, dihydropyridine or dihydropyrimidones acceptors *via* sequential GBB-3CR-Ugi-azide-4CR/Hantzsch-4CR/Biginelli-3CR synthesis.[6] Balijapalli and Iyer also designed imidazo[1,2-*a*]pyridine fluorophores exhibiting excited-state intramolecular proton transfer (ESIPT) properties, which were accessed in a copper-catalyzed three-component reaction rather than a GBB-3CR.[7] Due to their luminescence properties, we targeted the exploration of imidazo[1,2-*a*]heterocycles for different applications; e.g., pH sensing or DNA-staining.[8] To expand on these results, we envisioned imidazo[1,2-*a*]heterocycles acting as donor motifs in donor-acceptor chromophores that would emit *via* thermally activated delayed fluorescence (TADF).[9] In 2020, Lee *et al.* reported on the first series of TADF-emitters containing the imidazopyridine motif.[10] Nitrile groups were grafted onto the scaffold to enhance their electron-withdrawing properties and it was combined as an acceptor with two different donors. As the secondary amino substituent originating from the isonitrile employed in the GBB-3CR increases the electron density of the imidazopyridine, we expected that this moiety would be very

Table 1 Chemical Structures and DFT-Predicted Singlet-Triplet Energy Gaps and Vertical S_1 Energy Levels of the ImPy* Donor with Different Acceptor Types using the PBE0/6-31G(d,p) Method In Vacuum[a]

p-ImPy-CN	p-ImPy-NPI	p-ImPy-Ph.Bs.	p-ImPy-Baz	p-ImPy-Try	p-ImPy-Aq
0.92 eV	0.73 eV	0.65 eV	0.63 eV	0.40 eV	0.18 eV
3.95 eV (389 nm)	3.19 eV (389 nm)	3.62 eV (343 nm)	3.66 eV (339 nm)	3.43 eV (361 nm)	2.75 eV (450 nm)

[a] Top row: ΔE_{ST}, bottom row: S_1 energy

well suited as a donor rather than an acceptor. We thus targeted the design of donor-acceptor TADF-emitters featuring an ImPy-based donor.

Prior to synthesis, we assessed the feasibility of our design using density functional theory by partnering the 3-(*tert*-butylamino) imidazo[1,2-*a*]pyridine moiety with a range of electron-accepting groups that had previously been studied in donor-acceptor TADF emitters. We first modelled a set of potential structures with 3-*tert*-butyl imidazo[1,2-*a*]pyridine as the donor, a 2,6-dimethylphenylene bridge that is coupled at the 4-position to the acceptor motif (ImPy*). The results are listed in Table 1.

According to the calculations, the dihedral angle between the ImPy* unit and the 2,6-dimethylphenylene bridging unit is ca. 29°. The smallest ΔE_{ST} value was obtained for the combination of ImPy and anthraquinone (Aq). The ImPy-group acts as a relatively weak donor, thus pairing it with the strong acceptor anthraquinone was necessary to stabilize the S_1 energy into the visible regime and decrease the singlet-triplet energy gap, ΔE_{ST}, to a value where TADF may be possible. Coupling ImPy to weaker electron acceptors would yield a weaker charge-transfer state that would place the likely emission in the UV region.

Based on these results, we envisaged that incorporating multiple ImPy residues attached to a central phenylene spacer would effectively increase the strength of the charge-transfer S_1 state, red-shifting the emission and decreasing further ΔE_{ST}. A series of target emitters with different configurations of donors and the Aq acceptor was designed: *o*-, *m*-, and *p*-ImPyAq. The differing regiochemistry of the donor was expected to influence the exchange ener-

gy of the emitter and thus ΔE_{ST}. The energy levels of the frontier orbitals of the three isomers and their localization in the optimized structures are presented in Figure 1.

For all three proposed compounds, the estimated ΔE_{ST} values are moderately small, with *p*-ImPyAq* exhibiting the largest ΔE_{ST} of 0.18 eV while the bis-ImPyAq isomers both have predicted ΔE_{ST} of 0.10 eV. The LUMOs of each of the three structures are almost exclusively located on the anthraquinone acceptor, while the HOMOs span over the imidazo[1,2-*a*]pyridine moiety and the central phenylene ring. In the case of *p*-ImPyAq*, the greater extension of the LUMO onto the bridge explains the higher ΔE_{ST} for this compound. The HOMO-LUMO gaps were calculated to range from 2.78 to 3.11 eV. However, the singlet oscillator strength of all compounds is relatively low, reflecting the poor overlap of the electron densities of the HOMO and LUMO in each molecule.

To access the proposed structures starting from a set of donors and acceptors, a modular synthesis approach was developed by dissecting the emitters into individual building blocks. The donor building blocks, comprising the ImPy moiety and the phenylene spacer, were prepared *via* a GBB-3CR from the respective brominated benzaldehydes (Scheme 1). For the *para*-emitter, the location of the methyl groups on the phenylene spacer was inverted because the respective aldehyde component for the GBB-3CR synthesis of this building block is more easily available. The yield of the mono-imidazo[1,2-*a*]pyridine donor **4a** was significantly better than for the bis-imidazo[1,2-*a*]pyridines due to their additional reactive site and because of the steric congestion in the case of **4c**.
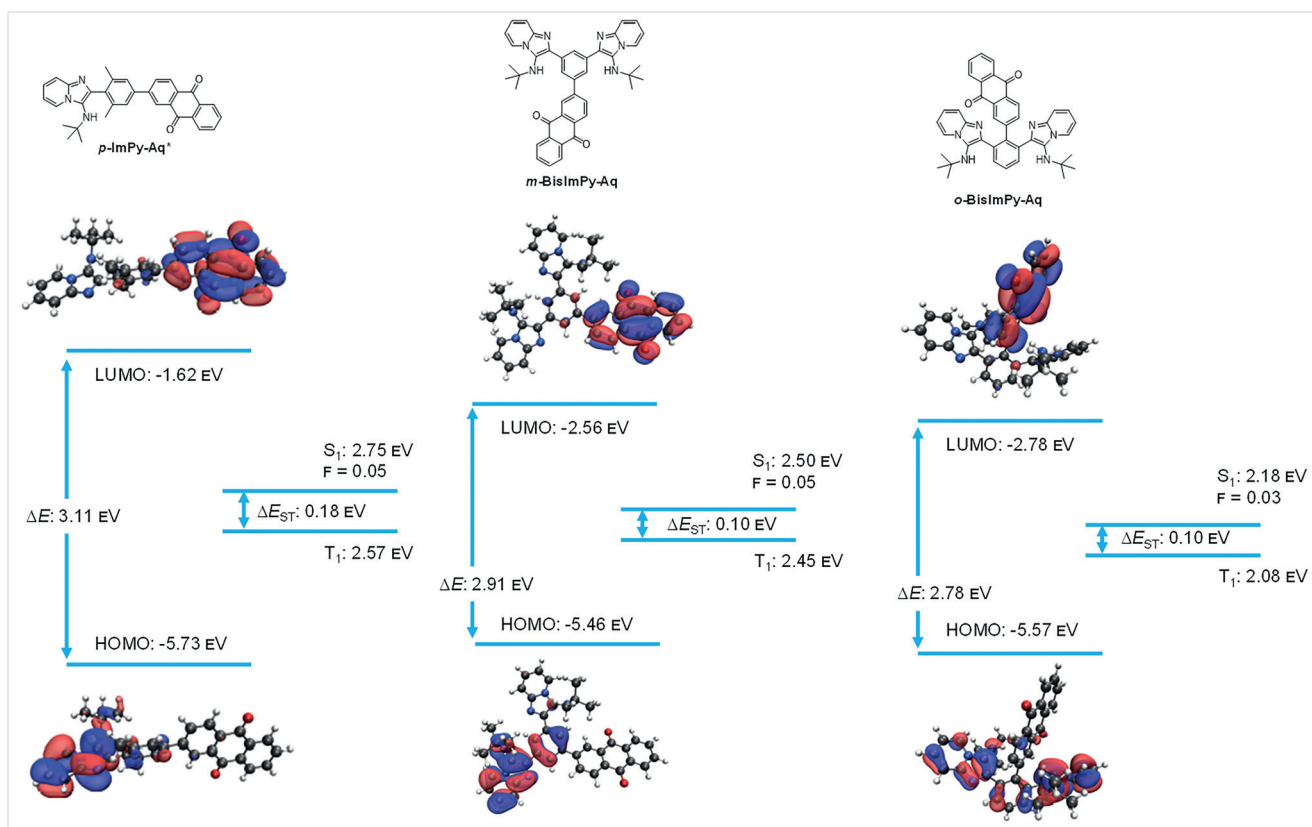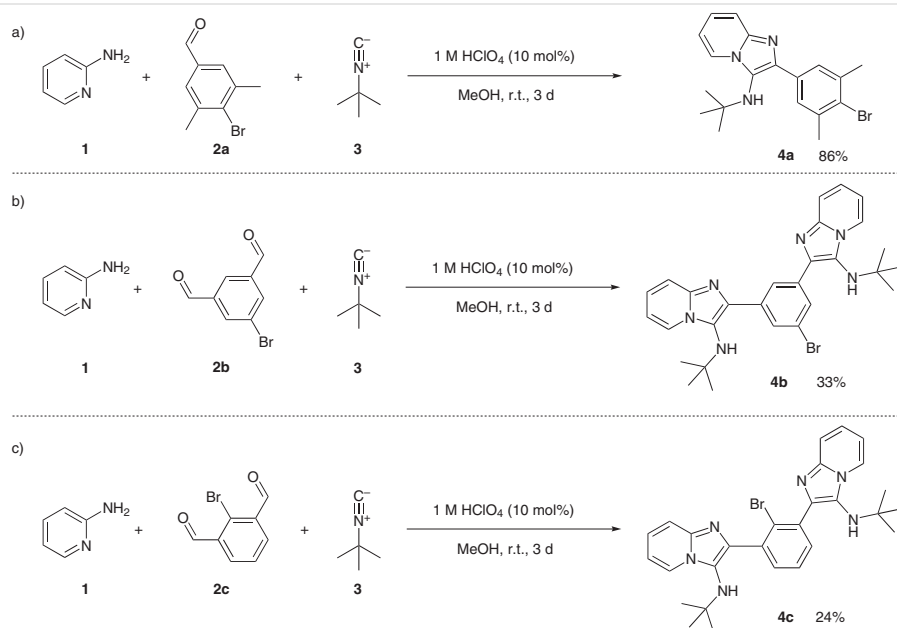
Figure 1 DFT-predicted HOMO and LUMO orbital distribution (isovalue 0.02) and singlet and triplet energies of *p*-ImPyAq*, *m*-BisImPyAq, and *o*-BisImPyAq using the PBE0/6-31G(d,p) method in vacuum.

Scheme 1 Synthesis of the ImPy-donor building blocks **4a–c** *via* GBB-3CRs

1036

Synlett   M. Stahlberger et al.   THIEME OPEN ACCESS   Cluster

The acceptor building block, anthraquinone pinacol borate was prepared *via* Miyaura borylation according to a procedure by Liu *et al.* using a Pd(dppf)Cl$_2$ catalyst and potassium acetate as the base.[11] The desired product **6** was obtained in quantitative yield (Scheme 2).
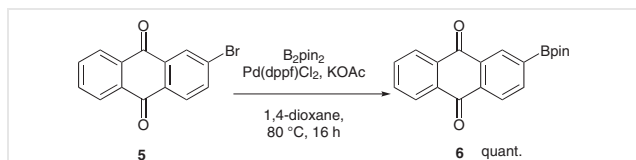

Scheme 2 Synthesis of anthraquinone pinacol borate **6** *via* Miyaura borylation

We next optimized the Suzuki–Miyaura conditions for the coupling of the individual building blocks to form the targeted donor-acceptor compounds. To find the best reaction conditions for this key step, we first optimized the synthesis of *p*-ImPyAq as a model system. The conversion of **4a** into **7** was calculated from the ^{1}H NMR spectra of the crude products to identify the most effective reaction conditions. For this, the ratio of the signals' integrals corresponding to the methyl residues of the phenyl spacer of both starting

material and product were used. As no internal standard was employed, the conversion does not reflect the actual isolated yield. The results are displayed in Table 2. Among the tested Pd sources, palladium(II) acetate performed best. Potassium acetate and potassium carbonate were used for the optimization of the Pd source and the ligand. The best results were obtained using RuPhos and SPhos (entries 9 and 11); without any ligand, only traces of the product could be detected (entry 12). Using stronger bases like potassium *tert*-butoxide, potassium hydroxide or cesium carbonate led to a significantly improved conversion as, in all three cases, no residual starting material was present (entries 13–15). Considering the overall purity of the product based on its ^{1}H NMR spectrum from each of the various entries, cesium carbonate was chosen. Using these optimized conditions, the target *ortho*-, *meta*- and *para*-emitters were synthesized from the respective building blocks (Scheme 3).

After flash chromatography, *p*-ImPyAq (**7**) was obtained in a yield of 61%.[12] The notable difference between the quantitative conversion of **4a** into **7** (see Table 2) and the isolated yield of **7** is due to losses during the compound's purification. For *m*-BisImPyAq (**8**), the yield was even high-

Table 2 Optimization of the Reaction Condition for the Suzuki–Miyaura Coupling of **4a** and **6**
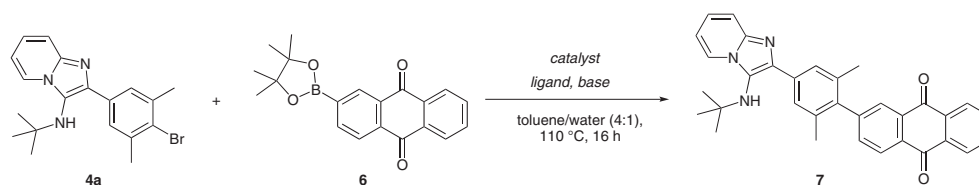
Entry	Catalyst	mol%	Ligand	mol%	Base	Conversion (%)[b]
1	Pd(dba)$_2$	5	XPhos	10	K$_2$CO$_3$	53
2	Pd$_2$(dba)$_3$	5	XPhos	10	K$_2$CO$_3$	44
3	Pd(PPh$_3$)$_4$	5	XPhos	10	K$_2$CO$_3$	62
4	Pd-Peppsi-iPr	5	XPhos	10	K$_2$CO$_3$	24
5	Pd(OAc)$_2$	5	XPhos	10	K$_2$CO$_3$	64
6	Pd(OAc)$_2$	10	XPhos	20	K$_2$CO$_3$	55
7	Pd(OAc)$_2$	2	XPhos	4	K$_2$CO$_3$	25
8	Pd(OAc)$_2$	5	XPhos	10	KOAc	39
9	Pd(OAc)$_2$	5	SPhos	10	KOAc	51
10	Pd(OAc)$_2$	5	CataCXium A	10	KOAc	36
11	Pd(OAc)$_2$	5	RuPhos	10	KOAc	51
12	Pd(OAc)$_2$	5	–	–	KOAc	3
13	Pd(OAc)$_2$	5	RuPhos	10	KO^{t}Bu	>99
14	Pd(OAc)$_2$	5	RuPhos	10	KOH	>99
15	Pd(OAc)$_2$	5	RuPhos	10	Cs$_2$CO$_3$	>99

^{a} Conditions: **4a** (1.00 equiv), **6** (1.10 equiv), catalyst, ligand, base (3.00 equiv), solvent: toluene/water (4:1), 110 °C, 16 h.
^{b} The conversion was calculated using the ratio of the ^{1}H NMR signals' integrals of **4a** and **7**.
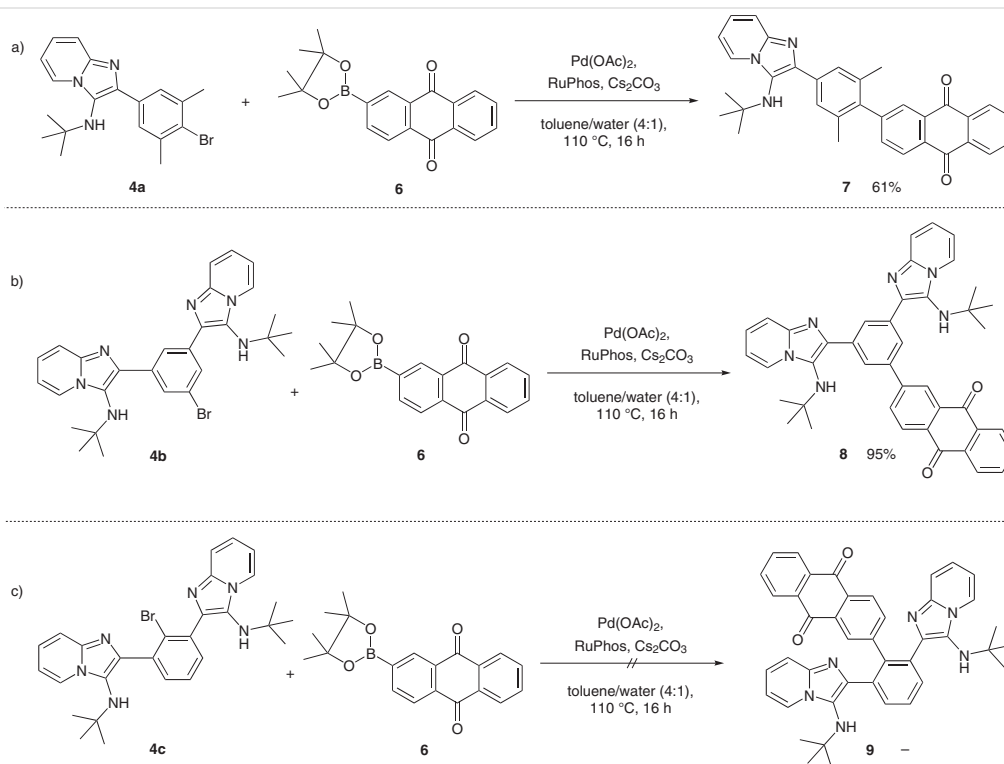
Scheme 3 Synthesis of the *ortho*-, *meta*-, and *para*-ImPyAq through Suzuki–Miyaura coupling of the donor and acceptor building blocks

er, at 95%, likely due to the reduced steric hindrance of the bromide.[13a] The structure of **8** was confirmed unambiguously through single-crystal X-ray crystallography (Figure 2).[13b]

On the other hand, *o*-BisImPyAq (**9**) could not be obtained. Instead, protodeboronation of the anthraquinone pinacol borate was observed while the ImPy building block
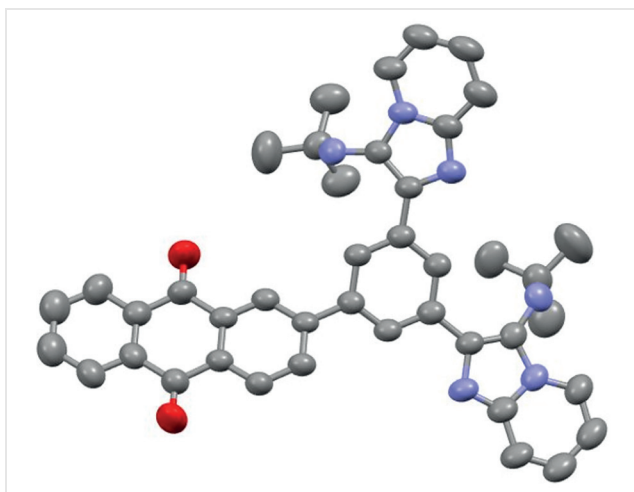

Figure 2 Molecular structure of one crystallographic independent molecule of **8** (displacement parameters are drawn at 50% probability level)

remained unconverted. Addressing positions between sterically hindered residues is quite challenging and only a few procedures have been reported; e.g., using AntPhos as a ligand. While this catalytic system is feasible for adjacent phenyl substituents, no reaction was observed for imidazo[1,2-*a*]pyridines. Hence, *o*-BisImPyAq needed to be accessed *via* a different route. Therefore, the acceptor unit was attached to the bridging aldehyde prior to the synthesis of the imidazo[1,2-*a*]pyridine moieties. The synthetic approach is depicted in Scheme 4.

2-Bromoisophthalaldehyde **2c** was coupled to anthraquinone pinacol borate **6** in a Suzuki–Miyaura reaction. The desired coupling product **10** was obtained in a yield of 19%. Presumably, the losses are due to side reactions like decarbonylation of the neighboring formyl groups as a significant evolution of gas was observed during the reaction. Subsequently, the formyl groups were transformed into 3-aminoimidazo[1,2-*a*]pyridines in a GBB-3CR. Initially, standard conditions were applied. However, even after a prolonged reaction time of ten days, the conversion remained incomplete. Thus, the solvent was changed to chloroform and the temperature was increased to 60 °C to accelerate the reaction. Through this modification to the reaction conditions, an excellent yield of 92% for **9** could be achieved.[14]

The synthesized compounds were studied to assess their photophysical properties and to evaluate whether the emitters exhibit TADF properties. For this, absorption and
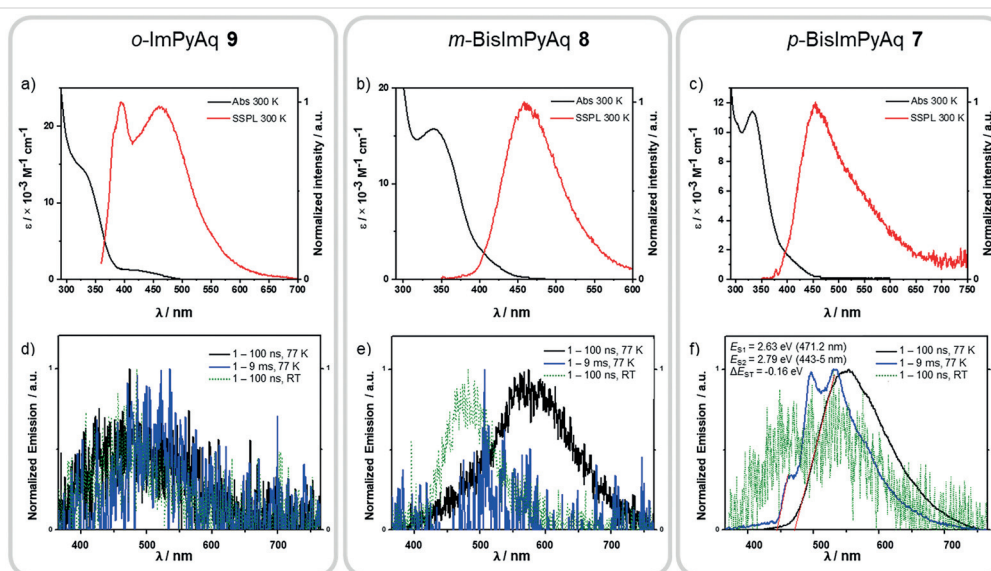
1038

Synlett   M. Stahlberger et al.   THIEME OPEN ACCESS   Cluster

Figure 3 (a–c) Absorption (black, obtained in toluene (1×10^{-5} M) at 300 K) and normalized emission spectra (red, obtained in toluene (1×10^{-4} M) at 300 K) of **9** (λ_{exc} = 350 nm), **8** and **7** (λ_{exc} = 340 nm for both) (from left to right) measured at r.t.; (d–f) Normalized emission spectra of **9**, **8** and **7** (from left to right) measured in toluene (10 µM, λ_{exc} = 343 nm) at different time scales and temperatures: 1–100 ns at 77 K (black), 1–9 ms at 77 K (blue), 1–100 ns at r.t. (green).

emission spectra of the compounds were recorded at ambient temperature (Figure 3a, Table 3), and emission at 77 K over different time scales (Figure 3b). The absorption spectra of all derivatives show similar profiles, with the highest intensity bands located at 290 nm, followed by lower intensity shoulders at 320–370 nm and a varying intensity low-energy band at >380 nm. Isomeric differences among the derivatives are most notably reflected in the energy and intensity of this lowest energy absorption band, with **9** showing the highest intensity. The DFT-predicted absorption spectra follow a similar trend (Figure S19), except that they are considerably red-shifted compared to the experimental

results. The molar absorptivity values, ε, of the band located at 320–370 nm for **9**, **8** and **7** are 13,664, 15,717 and 11,424 M^{-1} cm^{-1}, respectively. Turning to emission in toluene, the spectra were acquired at a considerably high concentration (1×10^{-4} M) due to their weak fluorescence intensity. Hence, all the samples showed weak, broad emission bands in the sky-blue region, with peak maxima, λ_{PL}, of 463, 460, and 455 nm for **9**, **8** and **7**, respectively. The weak emission correlates with DFT-predicted low oscillator strength values. In *o*-ImPyAq **9**, we noticed what appears to be dual emission with the second higher-energy peak at 394 nm. We have excluded its origin as being due to solvent Raman
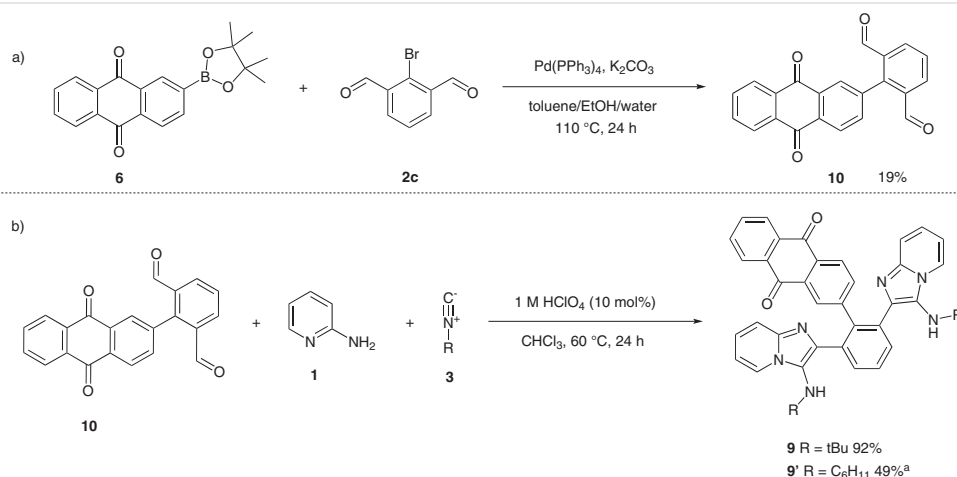
Scheme 4 Synthesis of (a) **10** and (b) **9** and **9'**. [a] The reaction was performed in MeOH at r.t. for 3 days.

1039

Synlett   M. Stahlberger et al.   THIEME OPEN ACCESS   Cluster

scattering as the scattering peak appeared at a higher energy, therefore this high-energy peak could be attributed to LE emission from one of the chromophores. There is a progressing bathochromic shift of the λ_{PL} from *para-* to *meta-* to *ortho-*isomers that is consistent with the trends predicted by TD-DFT; however, the experimentally observed emission red-shift is rather moderate (max. 8 nm). Low-temperature measurements were performed to investigate the fundamental luminescent mechanisms of the samples. For *o*-ImPyAq **9**, the signal-to-noise ratio remained poor, showing almost no emission at all. For *m*-ImPyAq **8**, a bathochromic shift was observed for the prompt fluorescence at 77 K. No delayed luminescence was observed.

Table 3 Photophysical Properties of the Synthesized Emitters[a]

entry	λ_{abs} (nm)	ε_{max} (M^{-1} cm^{-1})	λ_{PL} (nm)
o-BisImPyAq **9**	285 / 335	27,828 / 13,780	394, 463
m-BisImPyAq **8**	285 / 340	32,545 / 15,727	460
p-ImPyAq **7**	283 / 332	18,432 / 11,414	455

[a] Measured in toluene. λ_{exc} = 343 nm.

In contrast to this, the emission intensity of *p*-ImPyAq **7** was significantly increased upon cooling to 77 K. While at room temperature the compound was barely emissive, an intense green-yellowish prompt emission was observed at 77 K. Aside from the prompt fluorescence, a delayed luminescence was also observed. Surprisingly, the maximum emission wavelength of the delayed fluorescence showed a hypsochromic shift. A potential reason might be that the sample was flash-frozen, thus the conformations of the individual molecules are not in equilibrium.[15] The broad and structureless singlet emission shape hints at emission occurring from a charge-transfer state, while the structured phosphorescence is consistent with a locally excited emission from anthraquinone individual chromophores.[16] Similar behavior in flash-freeze luminescence experiments was also observed in other donor–acceptor systems.[15a]

In summary, a series of donor–acceptor chromophores bearing a 3-aminoimidazo[1,2-*a*]pyridine donor motif was synthesized through a GBB-3CR/Suzuki–Miyaura coupling sequence. While multicomponent methods are still underrepresented in the synthesis of functional materials, this study showcases the advantages of such modular approaches. The GBB-3CR offers facile access to the imidazo[1,2-*a*]scaffold, which can easily be derivatized through combinatorial variation of the individual components. This way, a series of ImPy-based building blocks with different geometries and substitution patterns were synthesized in overall good yields. Subsequently, these ImPy-building blocks can be coupled to a variety of acceptor moieties. With the optic of designing new TADF emitters, DFT calculations were used to assess a family of ImPy-acceptor compounds possessing different acceptors. This study revealed that in combination with an anthraquinone acceptor moiety, the calculated ΔE_{ST} values of the ImPy-based compounds were in a range suitable for TADF. However, spectroscopic and optoelectronic characterization only show very weak emission at ambient temperatures for the series of synthesized ImPyAq emitters. This is likely due to a combination of very low oscillator strength and competing non-radiative deactivation pathways. The detailed origin of this behavior is the subject of further studies. Thus, adjustments and optimizations of the structures are necessary to improve the optoelectronic properties of this class of emitters. Therefore, our modular approach lends itself perfectly to assess different combinations of donor and acceptor motifs. Overall, the ImPy-donor motive and the MCR-based synthesis concept provide a versatile synthetic platform for the development of new types and architectures of fluorescent emitters.

Conflict of Interest

The authors declare no conflict of interest.

Funding Information

Acknowledgment

Supporting Information

Supporting information for this article is available online at https://doi.org/10.1055/a-2236-8949.

Primary Data

The primary data and additional information on the chemical syntheses in this report are available via Chemotion repository: https://dx.doi.org/10.14272/collection/MSB_2023-07-12.
The research data supporting this publication can be accessed at https://doi.org/10.17630/85cd88f6-5e2f-4916-a8fd-b121ac024d61.

References and Notes

(1) Boltjes, A.; Dömling, A. *Eur. J. Org. Chem.* **2019**, 7007.
(2) Wolff, F. E.; Hofener, S.; Elstner, M.; Wesolowski, T. A. *J. Phys. Chem. A* **2019**, *123*, 4581.
(3) (a) Bienaymé, H.; Bouzid, K. *Angew. Chem. Int. Ed.* **1998**, *110*, 2349. (b) Blackburn, C.; Guan, B.; Fleming, P.; Shiosaki, K.; Tsai, S. *Tetrahedron Lett.* **1998**, *39*, 3635. (c) Groebke, K.; Weber, L.; Mehlin, F. *Synlett* **1998**, 661.
(4) (a) de Moliner, F.; Kielland, N.; Lavilla, R.; Vendrell, M. *Angew. Chem. Int. Ed.* **2017**, *56*, 3758. (b) Finney, N. S. *Curr. Opin. Chem. Biol.* **2006**, *10*, 238. (c) Levi, L.; Muller, T. J. *Chem. Soc. Rev.* **2016**, *45*, 2825. (d) Rocha, R. O.; Rodrigues, M. O.; Neto, B. A. D. *ACS Omega* **2020**, *5*, 972. (e) Vendrell, M.; Zhai, D.; Er, J. C.; Chang, Y. T. *Chem. Rev.* **2012**, *112*, 4391.
(5) Burchak, O. N.; Mugherli, L.; Ostuni, M.; Lacapere, J. J.; Balakirev, M. Y. *J. Am. Chem. Soc.* **2011**, *133*, 10058.
(6) Shahrisa, A.; Esmati, S. *Synlett* **2013**, *24*, 595.
(7) Balijapalli, U.; Iyer, S. K. *Dyes Pigm.* **2015**, *121*, 88.
(8) (a) Stahlberger, M.; Schwarz, N.; Hassan, Z.; Zippel, C.; Hohmann, J.; Nieger, M.; Bräse, S. *Chem. Eur. J.* **2022**, *28*, e202103511. (b) Stahlberger, M.; Steinlein, O.; Adam, C. R.; Rotter, M.; Hohmann, J.; Nieger, M.; Köberle, B.; Bräse, S. *Org. Biomol. Chem.* **2022**, 3598.
(9) (a) Endo, A.; Ogasawara, M.; Takahashi, A.; Yokoyama, D.; Kato, Y.; Adachi, C. *Adv. Mater.* **2009**, *21*, 4802. (b) Uoyama, H.; Goushi, K.; Shizu, K.; Nomura, H.; Adachi, C. *Nature* **2012**, *492*, 234. (c) Hong, G.; Gan, X.; Leonhardt, C.; Zhang, Z.; Seibert, J.; Busch, J. M.; Bräse, S. *Adv. Mater.* **2021**, *33*, e2005630.
(10) Kothavale, S.; Lee, K. H.; Lee, J. Y. *Chem. Eur. J.* **2020**, *26*, 845.
(11) Liu, S.; Zhang, H.; Li, Y.; Liu, J.; Du, L.; Chen, M.; Kwok, R. T. K.; Lam, J. W. Y.; Phillips, D. L.; Tang, B. Z. *Angew. Chem. Int. Ed.* **2018**, *57*, 15189.
(12) **Synthesis of *p*-ImPyAq (7):** Compound **4a** (111 mg, 298 μmol, 1.00 equiv), **6** (100 mg, 298 μmol, 1.00 equiv), Pd(OAc)₂ (3.36 mg, 14 μmol, 5 mol%), RuPhos (14 mg, 29 μmol, 1.00 equiv), and Cs₂CO₃ (293 mg, 89 μmol, 3.00 equiv) were dissolved in a mixture of toluene and water (4:1, 4 mL). The mixture was stirred argon atmosphere for 16 h at 110 °C. The solvent was removed under reduced pressure and the residue was purified *via* flash chromatography (SiO₂, CH/EtOAc 7:1 to 1:1). Compound **7** (91 mg, 182 μmol, 61%) was obtained as an orange solid.
Analytical data of 7: R_f = 0.43 (SiO₂, cyclohexane/EtOAc 1:1). ¹H NMR (500 MHz, CDCl₃): δ = 8.39 (d, *J* = 7.9 Hz, 1 H, CH$_{Ar}$), 8.35–8.31 (m, 2 H, CH$_{Ar}$), 8.23 (dt, *J* = 6.9, 1.2 Hz, 1 H, CH$_{Ar}$), 8.17 (d, *J* = 1.7 Hz, 1 H, CH$_{Ar}$), 7.82–7.78 (m, 2 H, CH$_{Ar}$), 7.76 (s, 2 H, CH$_{Ar}$), 7.65 (dd, *J* = 7.9, 1.7 Hz, 1 H, CH$_{Ar}$), 7.55 (dt, *J* = 9.0, 1.2 Hz, 1 H, CH$_{Ar}$), 7.13 (ddd, *J* = 9.0, 6.6, 1.3 Hz, 1 H, CH$_{Ar}$), 6.77 (td, *J* = 6.8, 1.2 Hz, 1 H, CH$_{Ar}$), 3.12 (br, 1 H, N*H*), 2.10 (s, 6 H, CH₃), 1.11 (s, 9 H, CH₃). ¹³C NMR (126 MHz, CDCl₃): δ = 183.5 (C$_q$, CO), 183.2 (C$_q$, CO), 148.0 (C$_q$), 142.2 (C$_q$), 139.1 (C$_q$), 139.0 (C$_q$), 135.5 (C$_q$), 135.4 (CH$_{Ar}$), 134.9 (C$_q$), 134.3 (C$_q$), 134.2 (CH$_{Ar}$), 134.2 (CH$_{Ar}$), 133.7 (2C, C$_q$), 132.2 (C$_q$), 128.3 (CH$_{Ar}$), 127.7 (CH$_{Ar}$), 127.4 (CH$_{Ar}$), 127.4 (CH$_{Ar}$), 127.3 (CH$_{Ar}$), 127.3 (2C, CH$_{Ar}$), 124.1 (CH$_{Ar}$), 123.7 (C$_q$), 123.6 (CH$_{Ar}$), 117.5 (CH$_{Ar}$), 111.4 (CH$_{Ar}$), 56.3 (C$_q$), 30.4 (3C, CH₃), 20.8 (2C, CH₃). IR (ATR): 2965 (w), 2921 (w), 1666 (vs), 1588 (s), 1445 (w), 1363 (w), 1343 (m), 1323 (s), 1299 (s), 1286 (s), 1268 (s), 1241 (s), 1214 (m), 1183 (m), 1159 (m), 1037 (w), 1031 (w), 1004 (w), 959 (w), 929 (s), 895 (w), 882 (m), 858 (m), 841 (w), 817 (w), 789 (w), 762 (vs), 741 (w), 731 (m), 710 (vs), 674 (m), 636 (w), 625 (w), 606 (w), 588 (m), 561 (w), 524 (w), 436 (m), 407 (m), 382 (m) cm⁻¹. FAB-MS: *m/z*

(%) = 500 (53), 155 (33), 154 (100), 138 (43), 137 (69), 136 (80), 107 (34), 95 (28), 91 (42). HRMS-FAB: *m/z* [M + H]⁺ calcd for C₃₃H₃₀O₂N₃: 500.2333; found: 500.2330.

(13) (a) **Synthesis of *m*-BisImPyAq (8):** Compound **4b** (557 mg, 1.05 mmol, 1.00 equiv), **6** (350 mg, 1.05 mmol, 1.00 equiv), RuPhos (48.9 mg, 105 μmol, 0.10 equiv), Cs₂CO₃ (1.02 g, 3.14 mmol, 3.00 equiv) and Pd(OAc)₂ (11.8 mg, 52.4 μmol, 0.05 equiv) were dissolved under argon atmosphere in a mixture of toluene and water (4:1, 25 mL) and stirred for 16 h at 110 °C. The solvent was removed under reduced pressure, and the residue was purified *via* flash chromatography (SiO₂, CH/EE 7:1 to 1:10). Compound **8** (656 mg, 995 μmol, 95%) was isolated as a red solid.
Analytical data of 8: R_f = 0.16 (SiO₂, cyclohexane/EtOAc 1:6). ¹H NMR (500 MHz, CDCl₃): δ = 8.71 (d, *J* = 1.9 Hz, 1 H, CH$_{Ar}$), 8.64 (t, *J* = 1.6 Hz, 1 H, CH$_{Ar}$), 8.41 (d, *J* = 8.1 Hz, 1 H, CH$_{Ar}$), 8.39–8.31 (m, 4 H, CH$_{Ar}$), 8.27 (dt, *J* = 6.9, 1.2 Hz, 2 H, CH$_{Ar}$), 8.23 (dd, *J* = 8.1, 2.0 Hz, 1 H, CH$_{Ar}$), 7.87–7.77 (m, 2 H, CH$_{Ar}$), 7.57 (dt, *J* = 9.0, 1.1 Hz, 2 H, CH$_{Ar}$), 7.17 (ddd, *J* = 9.0, 6.6, 1.4 Hz, 2 H, CH$_{Ar}$), 6.81 (td, *J* = 6.8, 1.2 Hz, 2 H, CH$_{Ar}$), 3.34 (s, 2 H, N*H*), 1.11 (s, 18 H, CH₃). ¹³C NMR (126 MHz, CDCl₃): δ = 183.4 (2C, C$_q$, CO), 183.2 (2C, C$_q$, CO), 147.2 (C$_q$), 142.3 (2C, C$_q$), 139.2 (2C, C$_q$), 139.1 (C$_q$), 136.4 (2C, C$_q$), 134.3 (CH$_{Ar}$), 134.2 (CH$_{Ar}$), 134.0 (C$_q$), 133.9 (C$_q$), 132.8 (CH$_{Ar}$), 132.3 (C$_q$), 128.5 (CH$_{Ar}$), 128.2 (CH$_{Ar}$), 127.4 (CH$_{Ar}$), 126.3 (2C, CH$_{Ar}$), 125.8 (CH$_{Ar}$), 124.3 (2C, CH$_{Ar}$), 124.1 (2C, C$_q$), 123.7 (2C, CH$_{Ar}$), 117.5 (2C, CH$_{Ar}$), 111.6 (2C, CH$_{Ar}$), 56.8 (2C, C$_q$), 30.6 (6C, CH₃). IR (ATR): 2965 (m), 2929 (w), 2904 (w), 2868 (w), 1732 (w), 1672 (vs), 1632 (w), 1591 (vs), 1504 (w), 1473 (w), 1460 (w), 1441 (w), 1390 (w), 1361 (vs), 1323 (vs), 1296 (vs), 1239 (s), 1215 (vs), 1201 (vs), 1162 (m), 1112 (m), 1044 (m), 975 (m), 931 (s), 887 (m), 853 (m), 795 (w), 754 (vs), 732 (vs), 711 (vs), 670 (s), 639 (s), 633 (s), 605 (s), 483 (s), 448 (s), 404 (s), 392 (s), 381 (s) cm⁻¹. FAB-MS: *m/z* (%) = 661 (19), 660 (55), 659 (100) [M + H]⁺, 658 (30), 602 (30), 601 (39), 546 (26), 545 (27), 484 (25), 483 (73), 441 (26). HRMS-FAB: *m/z* [M + H]⁺ calcd for C₄₂H₃₉O₂N₆: 659.3129; found: 659.3130. (b) CCDC 2283444 (**8**) contains the supplementary crystallographic data for this paper. These data can be obtained free of charge from The Cambridge Crystallographic Data Centre via www.ccdc.cam.ac.uk/data_request/cif.

(14) **Synthesis of *o*-BisImPyAq (9):** 2-Aminopyridine (41.5 mg, 440 μmol, 2.00 equiv), **10** (75 mg, 220 μmol, 1.00 equiv), *tert*-butyl isonitrile (36.6 mg, 50 μL, 440 μmol, 2.00 equiv) and a solution of perchloric acid in methanol (1 M, 4.42 mg, 44 μL, 44.0 μmol, 0.20 equiv) were dissolved in chloroform and stirred at 60 °C for 1 d. The solvent was removed under reduced pressure, and the residue was purified *via* flash chromatography (SiO₂, CH/EtOAc 5:1 to 1:10). Compound **9** (134 mg, 203 μmol, 92%) was isolated as an orange solid.
Analytical data of 9: R_f = 0.06 (SiO₂, CH/EtOAc 1:6). ¹H NMR (500 MHz, CDCl₃): δ = 8.71 (d, *J* = 1.9 Hz, 1 H, CH$_{Ar}$), 8.64 (t, *J* = 1.6 Hz, 1 H, CH$_{Ar}$), 8.39–8.31 (m, 4 H, CH$_{Ar}$), 8.30–8.17 (m, 4 H, CH$_{Ar}$), 7.87–7.78 (m, 2 H, CH$_{Ar}$), 7.57 (dt, *J* = 8.9, 1.1 Hz, 2 H, CH$_{Ar}$), 7.25–7.13 (m, 2 H, CH$_{Ar}$), 6.80 (td, *J* = 6.8, 1.2 Hz, 2 H, CH$_{Ar}$), 3.35 (s, 2 H, N*H*), 1.10 (s, 18 H, CH₃). ¹³C NMR (126 MHz, CDCl₃): δ = 182.9 (C$_q$, CO), 181.9 (C$_q$, CO), 147.0 (C$_q$), 142.6 (2C, C$_q$), 139.3 (C$_q$), 137.7 (C$_q$), 136.2 (CH$_{Ar}$), 135.2 (2C, C$_q$), 134.2 (2C, C$_q$), 134.2 (2C, CH$_{Ar}$), 133.7 (CH$_{Ar}$), 133.5 (C$_q$), 133.4 (C$_q$), 133.1 (C$_q$), 132.5 (2C, C$_q$), 131.7 (CH$_{Ar}$), 129.1 (CH$_{Ar}$), 128.9 (CH$_{Ar}$), 127.5 (CH$_{Ar}$), 127.3 (CH$_{Ar}$), 127.0 (CH$_{Ar}$), 124.6 (C$_q$), 124.4 (2C, CH$_{Ar}$), 123.5 (2C, CH$_{Ar}$), 117.4 (2C, CH$_{Ar}$), 111.4 (2C, CH$_{Ar}$), 56.7 (2C, C$_q$), 30.6 (6C, CH₃). IR: 3369 (w), 2958 (w), 2924 (w), 2854 (w), 1672 (vs), 1630 (w), 1591 (m), 1554 (w), 1550 (w), 1500 (w), 1473 (w), 1455 (w), 1441 (w), 1388 (w), 1364 (m), 1339

(m), 1322 (s), 1299 (vs), 1266 (m), 1242 (m), 1221 (s), 1211 (s), 1198 (s), 1173 (m), 1146 (w), 1135 (w), 1081 (w), 972 (w), 962 (w), 952 (w), 931 (m), 907 (w), 857 (m), 817 (m), 756 (vs), 737 (vs), 710 (vs), 673 (m), 646 (w), 633 (w), 612 (w), 572 (w), 458 (w), 428 (w), 401 (w), 382 (s) cm^{-1}. FAB-MS: m/z (%) = 665 (43), 664 (100), 662 (42), 661 (31), 660 (46), 659 (85), 658 (30), 648 (31), 647 (67), 530 (73), 219 (83), 191 (33), 163 (31), 161 (32), 159 (30), 154 (41), 149 (32), 147 (61), 136 (41), 131 (38), 119 (34), 107 (37), 105 (43), 97 (38), 95 (53), 91 (71). HRMS-FAB: m/z [M + H]$^+$ calcd for $C_{42}H_{39}O_2N_6$: 659.3129; found: 659.3127.

(15) (a) Gupta, A. K.; Matulaitis, T.; Cordes, D. B.; Slawin, A. M. Z.; Samuel, I. D. W.; Zysman-Colman, E. *Can. J. Chem.* **2022**, *100*, 224. (b) Sun, D.; Saxena, R.; Fan, X.; Athanasopoulos, S.; Duda, E.; Zhang, M.; Bagnich, S.; Zhang, X.; Zysman-Colman, E.; Köhler, A. *Adv. Sci.* **2022**, *9*, 2201470.

(16) Carlson, S. A.; Hercules, D. M. *J. Am. Chem. Soc.* **1971**, *93*, 5611.